Effect of atmospheric condition on the thermal decomposition kinetics and thermodynamics of lead acetate trihydrate

Gülbanu Koyundereli ÇILGI

Manisa Celal Bayar University, Faculty of Engineering, Department of Metallurgy and Materials Engineering,
Campus of Şehit Prof. Dr. İlhan Varank, 45140, Manisa, Turkey

E-mail: gulbanu.cilgi@cbu.edu.tr

In this study thermal decomposition routes and kinetics of lead acetate triydrate are compared in inert (nitrogen) and reactive (oxygen) atmospheres by using thermogravimetric method. The decomposition proceeds with five consecutive stages in the both the atmospheres. The first four stages occur similarly in nitrogen and oxygen atmospheres and the same intermediates are formed. However, the last stage, differs according to the furnace atmosphere. The mixture of PbO and small amount metallic Pb is the final product in nitrogen atmosphere whereas the mixture of PbO and Pb_3O_4 is the final product in oxygen atmosphere. X-ray powder diffraction method is used in identify of these products. Kinetic calculations of all stages are realized by using Kissinger–Akahira–Sunose (KAS) and Flynn–Wall–Ozawa (FWO) model free methods. These methods are combined with modeling equations to find the effective model and to calculate thermodynamic parameters. It is found that all reactions show good harmony with the nucleation models although their indexes are different.

Keywords: Activation energy, Heterogeneous reactions, Lead acetate, Thermal decomposition, Thermodynamic parameters

Experimental factors, such as atmospheric condition, heating rate, particle size, sample mass are very important in thermal decomposition of solids. Especially atmospheric condition may cause differentiation of intermediate and final products. Cetişli et al.[1] investigated thermal and kinetic analysis of uranyl oxalate in nitrogen and oxygen atmospheres and found that final products (U_2O_5 and U_3O_8, respectively), activation energy values, decomposition models and thermodynamic parameters were different. Nakano et al.[2] compared thermal decomposition reactions of silver acetate in flowing helium and helium-oxygen mixture (21% oxygen) atmospheres and determined evolved gases by using mass spectra. In helium atmosphere; endothermic peak was observed in DTA curve and the peaks of evolution gases were detected in mass spectra at m/z = 59, 58, 43, 28, and 17. These peaks correspond to acetic acid, acetone, carbon dioxide, carbon monoxide and water, respectively. In helium-oxygen atmosphere, the peaks which belong to evolution of acetic acid and acetone disappeared in the mass spectra. Also, decomposition reaction observed with exothermic peak in DTA curve. These findings indicate that these organic gases combusted after evolution.

The calculations of kinetic and thermodynamic parameters of heterogeneous thermal decomposition reactions are very difficult due to a large number of complications. For instance, there is an interface between the reacting phases, and after formation of stable nuclei and their growth above the critical size, some (or all) of the following steps take place: mass transfer to the interface, reaction at the boundary, mass transfer of the products away from the interface or grain boundary movement, and heat transfer to or from the boundary[3-5].

Thermal decomposition of metal acetates have been studied for many years. Authors have aimed to obtain metal and metal oxide residues which have industrial importance such as catalysts, semiconductors, sensor etc. These studies have been limited to identification of intermediate and final products and determination of reaction temperature ranges. Detailed kinetic and thermodynamic calculations have not been realized[6-8].

The lead oxide is well-known with four basic types which are PbO, PbO_2, Pb_2O_3, and Pb_3O_4. Among them, lead dioxide (PbO_2) has the most common application fields because of the excellent chemical stability in an acidic medium[9]. It has been used as electrodes in electrochemical devices[10-11].

Furthermore, it has been preferred as a doped metal oxide-film electrode for the rapid degradation of organic compounds to CO_2 in wastewater[12]. Pb_3O_4, which is the other type of lead oxide, shows interesting physicochemical characteristics, because of its mixed valence of Pb ions and unique electronic structure. The usage of this oxide, as an anti-corrosive paint, as an electrode in batteries, and as a selective oxidant material has been studied by Zhou[13].

Mohamed et al.[14] investigated thermal decomposition of lead acetate trihydrate in nitrogen and dry air atmospheres from room temperature to 450°C. Authors identified intermediate and final products with using X-ray powder diffraction and IR transmission spectroscopy methods and emphasized that final products were differ in both atmospheres. The mixture of PbO and small amount of lead metal were final product in nitrogen atmosphere whereas only PbO was final product in dry air atmosphere. Researchers realized limited kinetic study with using Kissinger method and calculated activation energy values without any statistic data. Furthermore, any kinetic modeling or detailed thermodynamic calculations such as activation entropy, Gibbs free energy were not studied. Kinetic and thermodynamic findings play an important role in solid state physics and theoretical chemistry. However, there has been limited research effort devoted to thermal decomposition of lead acetate. So, there is a gap in the academic literature about kinetic analysis of each decomposition stage of lead acetate.

In this study, it is aimed to fill this deficiency in the academic literature and focused on kinetic and thermodynamic calculations. Thermogravimetric analysis of $Pb(CH_3COO)_2.3H_2O$ were studied in flowing nitrogen and oxygen atmospheres. Decomposition stages were identified and temperature ranges were determined by evaluating not only thermograms, but also minimum points of variation of activation energy versus decomposition fraction as shown in kinetic analysis section. Previously, activation energy values of each stage were calculated by using KAS (Kissinger-Akahira-Sunose) and FWO (Flynn–Wall–Ozawa) model-free equations. The graphs, which show the variation of activation energy with decomposition ratio, were prepared. Subsequently, the kinetic models of each stage were investigated. Thirteen model equations, which are well known in academic literature[15] were tested. The most proper model was selected. This model has the lowest standard deviation, the best regression analysis

value and the activation energies obtained from the modeling that are compatible with those obtained from model free KAS and FWO methods. Thermodynamic functions of activated complexes ($\Delta S^{\neq}$, $\Delta H^{\neq}$ and $\Delta G^{\neq}$) were calculated with using this model.

Experimental Section

$Pb(CH_3COO)_2.3H_2O$, which was purchased from Sigma Aldrich, was used without further purification. Thermogravimetry (TG), Differential Thermogravimetry (DTG), and Differential Thermal Analysis (DTA) measurements were performed by using a Shimadzu DTG-60H Simultaneous Thermal Analyzer. Temperature and mass calibrations are very important for the thermal analyzer systems and must be realized at the beginning of the experiments. Mass calibration was realized by using standard Shimadzu silver weights. Temperature calibration was performed by controlling the melting points of the tin and indium metals which were provided by Shimadzu. Flowing nitrogen and flowing oxygen atmospheres were selected as furnace atmosphere and flow rates were set at 100 mL min⁻¹. Samples were heated to 600°C with using 2, 4 and 6 °C min⁻¹ heating rates. The lower heating rates were preferred for separation of each reaction boundary clearly. Thus the initial and final temperatures of each reaction were determined more precisely. Additionally, the lower heating rates provided enough time to completion of the reactions and removal of the volatile products from the solid material. Highly sintered Al_2O_3 was selected as a reference material and measurements were carried out in alumina crucible. All experiments were repeated three times to reduce experimental errors and test reproducibility. The results showed that the reproducibility was high and the standard deviation was ±5 kJ/mol. The X-Ray powder diffraction patterns of residues were obtained with Bruker D8 Discover XRD, using CuKα (λ = 0.1542 nm) radiation source.

Kinetic calculations were realized by using model free KAS[16] and FWO[17] methods which were known "isoconversional methods" at the beginning of the studies. These methods do not assume any model or mechanism to calculate of activation energy. These methods are based on the fact that, reaction mechanism is not changed with decomposition ratio, temperature and heating rate and remain constant during the decomposition stage. With the use of these methods, the variation of the activation energy versus

decomposition ratio can be easily monitored. Therefore, it is preferred by many researchers[18-21]. The final equations of these methods are given below:

KAS : $ln\ \frac{\beta}{T^2} = \left[ln\ \frac{AR}{g(\alpha)E}\right] - \frac{E}{R}\cdot\frac{1}{T}$

FWO: $ln\ \beta = \left[ln\ \frac{AR}{g(\alpha)R}\right] - 5.3305 - 1.05178\frac{E}{R}\cdot\frac{1}{T}$

where, α corresponds to the degradation ratio (α= $(w_i-w_t)/(w_i-w_f)$), A stands for the pre-exponential factor, E denotes the activation energy, g(α) represents the differential conversion function, and R is the gas constant.

For each selected α constant, $ln\beta/T^2$ versus 1/T (KAS method) and lnβ versus 1/T (FWO method) were plotted. Activation energy values were calculated from the slope data of these graphs. The graphs between decomposition ratio and activation energy variation were plotted and discussed.

The most effective models were investigated and thermodynamic parameters of activated complexes were calculated at the continuation of the kinetic calculations. For this purpose KAS and FWO equations were rearranged as followings. These new methods are called as Composite Method I (C.M I) and Composite Method II (C.M II) in academic literature[22-24].

Modeling KAS equation- C.M I: $ln\ \frac{g(\alpha)}{T^2} = \left[ln\ \frac{AR}{\beta E}\right] - \frac{E}{R}\cdot\frac{1}{T}$

Modeling FWO equation-C.M II: $ln\ g(\alpha) = \left[ln\ \frac{AR}{\beta R}\right] - 5.3305 - 1.05178\frac{E}{R}\cdot\frac{1}{T}$

The values of $ln[g(\alpha)/T^2]$ (in modeling with KAS method) or $ln[g(\alpha)]$ (in modeling with FWO method) for different α value at a single β value were calculated and plotted versus 1/T values. The activation energy and pre-exponential factor values were calculated from the slope and intercept values respectively. Similar calculations were realized according to thirteen different theoretic model functions, g(α), which are well known in academic literature[15,25,26]. The most proper model, which has the lowest standard deviation, the best regression analysis value and the activation energies obtained from the modeling that are compatible with those obtained from model free KAS and FWO methods, was selected. $\Delta S^{\neq}$, $\Delta H^{\neq}$ and $\Delta G^{\neq}$ values of the activated complexes were calculated using activated complex (transition state) theory. Related equations were given below respectively.

$A = (e\chi kT_{avg.}/h).e^{\Delta S^{\neq}/R}$
$\Delta H^{\neq} = E_a - RT_{avg.}$
$\Delta G^{\neq} = \Delta H^{\neq} - T_{avg.}.\Delta S^{\neq}$

where e is the Neper number (2.7183), χ is the transition factor, which is unity for monomolecular reactions, k corresponds Boltzmann constant (1.381×10^{-23} J.K^{-1}), h denotes the Planck's constant (6.626×10^{-34} J.s), $T_{avg.}$ represents to the average reaction temperature and E_a stands for the activation energy which is calculated from the slope of Composite Methods graphs for the selected model.

Results and Discussion

Thermal (TG-DTG-DTA) analysis

The DTA and TG curves in both atmospheres, which were obtained with using 6 °C.min^{-1} heating rate, were given in Fig. 1a and 1b. The decomposition of lead acetate trihydrate completes within five stages in both atmospheres. First two stages correspond to dehydration reactions. These reactions occur consecutively and include difficulties to distinguish of each dehydration boundary. To make a more precise distinction, the activation energies of the combination of these two dehydrations were calculated and variation of activation energy versus dehydration ratio graph was prepared. Minimum point at this graph showed the moment when the first dehydration stage ended and the second stage began. This method was published academic literature previosly[27,28]. The details of this process are given in the kinetic results section.

Dehydration I (Dh.I), which advances removal of 2.25 mol crystal water, completes with 10.45% weight loss in nitrogen atmosphere and 10.64% weight loss in oxygen atmosphere. Second dehydration stage corresponds to removal of 0.75 mol crystal water. Experimental weight loss values of this stage are 2.62% and 2.53% in nitrogen, and oxygen atmospheres, respectively. Total experimental weight loss of these two stages (13.07% in nitrogen atmosphere and 13.18% in oxygen atmosphere) are lower than the corresponding theoretical value (14.25%). As seen from the Fig. 1, temperature differences between sample and reference (ΔT) in the DTA curves (Fig 1a) and mass loss in the TG curves (Fig. 1b) start immediately at the room temperature. These data show that dehydration begins suddenly at room temperature. Thus, the compound may have lost a small part of the water in the storage conditions. The similar situation is emphasized in the manuscript,
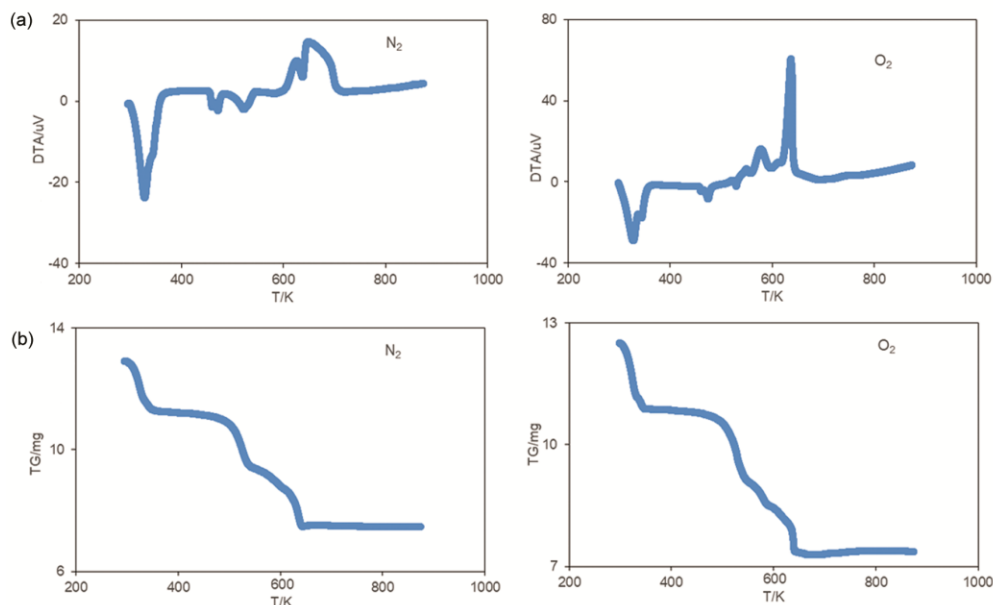
Fig. 1 — (a) DTA and (b) TG curves $Pb(CH_3COO)_2.3H_2O$ at 6 ^oC/min heating rate in the nitrogen and oxygen atmospheres

which was published by Mohamed et al.[14] and total dehydration weight loss was given as 11.64%.

Dehydration enthalpy values were calculated by using peak areas of the DTA curves at all heating rates. Average enthalpy value of Dh.I, was calculated as 135.75 kJ.mol^{-1} in nitrogen atmosphere and 121.67 kJ.mol^{-1} in oxygen atmosphere. If these enthalpy values are arranged to per mol water, results will be as 60.33 kJ.mol^{-1}.water^{-1} and 54.08 kJ.mol^{-1}.water^{-1} respectively. Dehydration II (Dh.II) requires lower enthalpy compared to Dh.I. Average enthalpy values of this stage are 24.97 kJ.mol^{-1}.water^{-1} in nitrogen atmosphere and 23.41 kJ.mol^{-1}.water^{-1} in oxygen atmosphere.

Anhydrite lead acetate preserves thermal stability till to 460 K and after this temperature, compound melts. The peak temperature value of melting reaction is compatible with academic literature[14]and it was measured as 470.41 K and 472.08 K in nitrogen and oxygen atmospheres, respectively. Decomposition reactions start immediately after the melting and advancing within three consecutive stages in both atmospheres. Activation energy-decomposition ratio graph of combined three decomposition stages was prepared to distinguish of each decomposition boundaries. The minimum points at this graph were considered as final point of first decomposition and the initial point consecutive decomposition.

As can be seen from Fig. 1a, all three decomposition stages show endothermic character in nitrogen atmosphere, whereas only the first decomposition stage shows endothermic character, second and third stages occur exothermically in oxygen atmosphere. $Pb(CH_3COO)_2.PbO$ occurs an intermediate decomposition product, at the end of the first decomposition stage in both atmosphere. This stage completes with 13.01% weight loss in nitrogen atmosphere and 14.68% weight loss in oxygen atmosphere. Second decomposition belongs to formation of $Pb(CH_3COO)_2.2PbO$ intermediate product in both atmosphere. Decomposition reaction occurs with endothermic process in the nitrogen atmosphere. Reaction peak observes from DTA curves and like a shoulder at 573.81 K averagely. This stage shows exothermic character in oxygen atmosphere and gives sharp peak at the DTA curve (Fig. 1a). Final oxide products are formed in the third decomposition step. The decomposition residues, which were identified by using X-Ray Powder Diffraction method, are different in both atmospheres. In nitrogen atmosphere, the final residue is composed of PbO and a small percentage of metallic Pb[29]. The experimental weight loss (42.18%) is partially higher than the theoretical weight loss (according to only PbO residue: 41.16%). This finding confirms that the final residue is not only PbO, but also includes small amount metallic Pb. In oxygen atmosphere, the final residue is composed of PbO and Pb_3O_4[30]. As seen from the Fig. 1b, weight gain (approx. 0.62%) is observed at the 667-768K temperature range and proves to oxidation of PbO to Pb_3O_4. X-Ray powder diffraction patterns of the final residues were given in Fig. 2.

Fig. 3, shows the effect of heating rate on the TG and DTA curves. The experiments were carried out in nitrogen atmosphere and the heating rates were varied to 2, 4 and 6 °C.min⁻¹, respectively. As expected, the reactions shifted to higher values with increasing heating rate. Heat transfer difficulties begin with the increase of the heating rate. A homogeneous temperature may not be achieved on all sides of the sample. Therefore, the reactions shift to higher temperatures. Same effect was observed in the other thermal analysis in the academic literature[31].

Kinetic results

KAS and FWO model free methods are used to investigate of activation energy-decomposition ratio variation at the beginning of the kinetic studies. The minimum points of this variation graphs indicate the
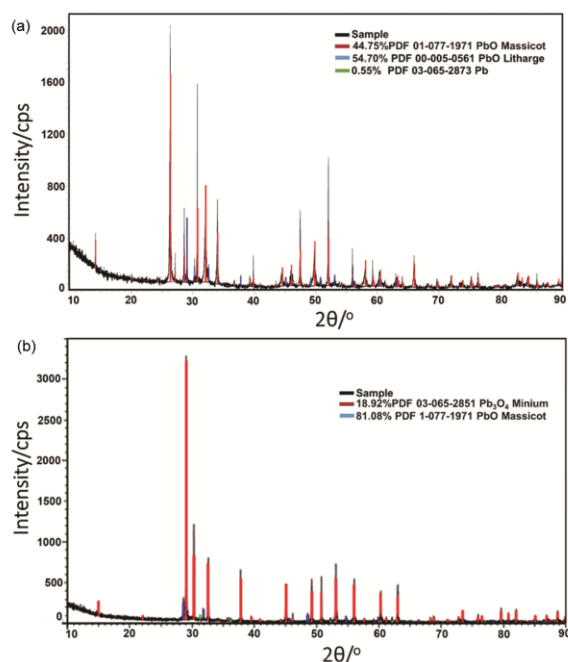
Fig. 2 — X-ray powder diffraction patterns of the final residues (a: in the nitrogen atmosphere and b: in the oxygen atmosphere)
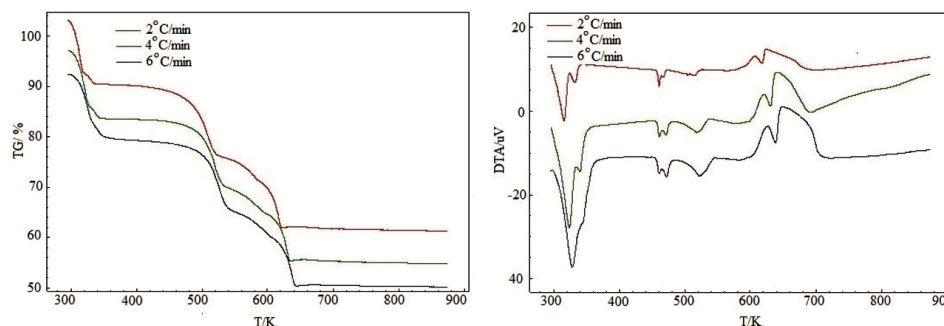
final point of first reaction and the initial point of consecutive second reaction. To distinguish boundaries of each dehydration stage; activation energy values of the combination two consecutive dehydrations were calculated and E_a-α variation graphs were prepared.

As seen from the Fig. 4a, activation energies reach the minimum values at $\alpha=0.808$ and $\alpha=0.804$ dehydration ratio in nitrogen and oxygen atmospheres respectively. The temperature and time values at these points were used and reaction boundaries of two consecutive dehydrations were determined. After that border separation, the activation energy values of each dehydration stage were calculated and the variations with respect to dehydration ratio, α, were graphed in Fig. 4b and Fig. 4c. Dh. I reaction requires high energy initially, but this requirement gradually decreases with progress of the reaction. Average activation energies were calculated as 77.481 and 82.714 kJ/mol in nitrogen and oxygen atmospheres respectively.

E_a-α variation of Dh.II in nitrogen atmosphere is slightly different compared to oxygen atmosphere (Fig. 4c). In nitrogen atmosphere, activation energies increase with advance of the dehydration and reach maximum (64.911 kJ/mol avg.) at $\alpha=0.60$ and then decrease consistently. The average activation energy values, which were calculated by using KAS and FWO methods, are 54.920 and 57.546 kJ/mol respectively. In oxygen atmosphere, activation energies increase with advance of the dehydration till to $\alpha=0.80$ and then decrease partially. The average activation energy values are higher (72.104 and 73.840 kJ/mol by using KAS and FWO methods respectively) compared to nitrogen atmosphere.

After these model free calculations, the reaction models were investigated by using C.M I and C.M II methods. The most proper reaction models were selected according to the evolution of regression

Fig. 3 — The TG and DTA curves of $Pb(CH_3COO)_2.3H_2O$ in the nitrogen atmosphere, at different heating rates
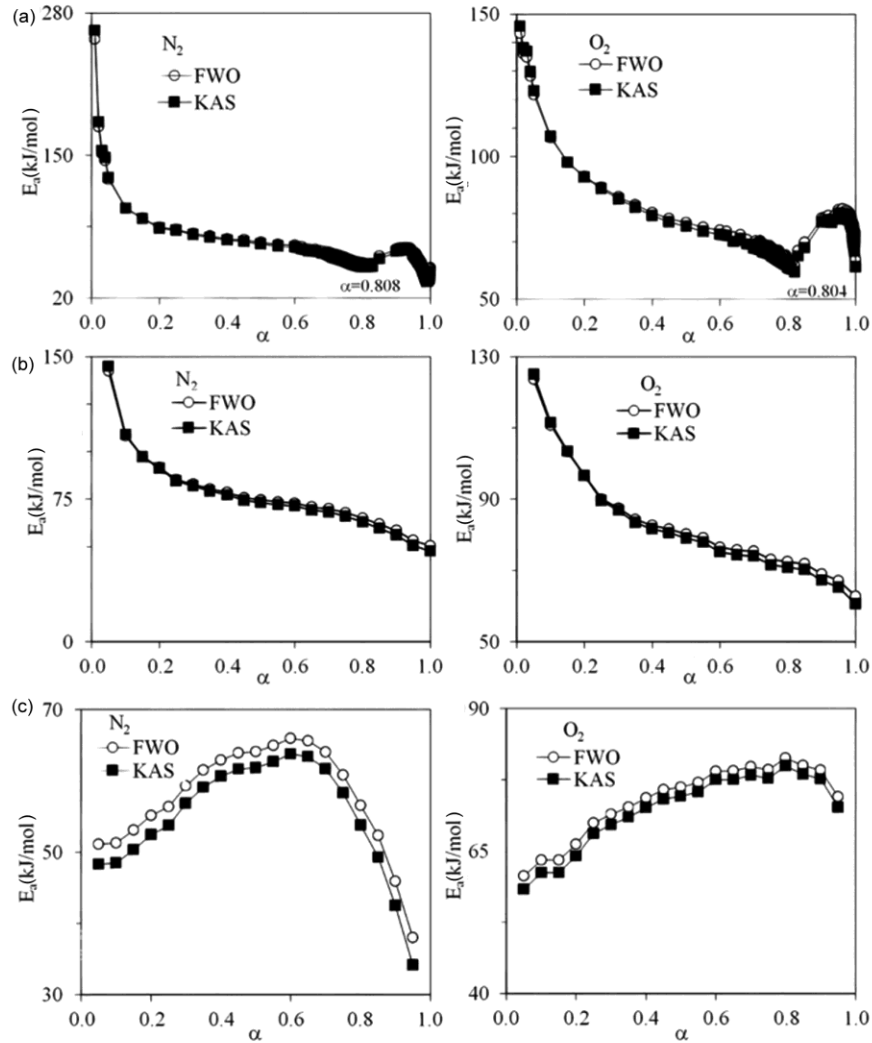
Fig. 4 — E_a-α variation graphs of dehydration reactions (a: combined dehydration reactions, b: dehydration I, c: dehydration II)

analysis and standard deviation data. In addition the harmonies between activation energies, which were calculated by using model free and modeling methods, were taken into account. Table 1 gives first two models that best fit to Dh.I and Dh.II reactions with their regression analysis, standard deviation and activation energy data. Activation energy values, which were calculated model-free KAS and FWO equations, were also presented in the same table for comparison.

As seen from the Table 1, nucleation and growth models are effective for Dh.I and Dh.II reactions in both atmospheres. Only nucleation indexes show differences depending on the dehydration stage and atmospheric conditions. The advances of dehydration reactions were explained by using nucleation and growth model commonly in academic literature[32,33].

After the determination of dehydration models, thermodynamic parameters of activated complexes were calculated. Results are given in Table 2.

The activation entropy ($\Delta S^{\neq}$) values of each dehydration stages are negative in the both atmospheric conditions. This situation shows that the corresponding activated complexes have higher degree of arrangement compared to the initial states. So, dehydration stages of lead acetate trihydrate compound may be interpreted as slow reactions[34,35]. Anhydrite compound shows thermal stability till to 460 K. After this temperature, it melts firstly without any mass loss and then decomposes to correspond residues (in nitrogen atmosphere: PbO and a small percentage of metallic Pb and in oxygen atmosphere: 81.08% PbO and 18.92 % Pb_3O_4 mixture) with three consecutive reactions. These reactions occur

Table 1 — The regression analysis, standard deviation and activation energy data of the first two models that best fit to dehydration (Dh I, Dh II) and decomposition (Dc I, Dc II, Dc III) reactions

	React.	Atmospheric condition	Method	Model	E_a (kJ/mol)	ln A	$\Delta H^{\#}$ (kJ/mol)	$\Delta S^{\#}$ (J/mol.K)	$\Delta G^{\#}$ (kJ/mol)
Dehydration	Dh. I	N₂	C.M I	A_2	65.88	23.71	63.25	-48.28	78.70
			C.M II	A_2	67.61	24.50	64.98	-41.74	78.34
		O₂	C.M I	A_2	67.95	24.59	65.32	-40.97	78.38
			C.M II	A_2	69.56	25.31	66.93	-34.99	78.10
	Dh.II	N₂	C.M I	A_4	51.27	16.70	48.47	-107.10	84.42
			C.M II	A_4	54.04	18.06	51.24	-95.81	83.39
		O₂	C.M I	A_3	71.53	24.59	68.75	-40.97	71.53
			C.M II	A_3	73.26	25.10	70.48	-37.15	82.72
Decomposition	Dc. I	N₂	C.M I	$A_{1.5}$	95.77	20.48	91.51	-79.17	131.90
			C.M II	$A_{1.5}$	99.031	21.43	94.77	-71.23	131.11
		O₂	C.M I	$A_{1.5}$	78.57	16.08	74.28	-115.76	133.69
			C.M II	$A_{1.5}$	82.74	17.42	78.45	-104.60	132.13
	Dc.II	N₂	C.M I	$A_{1.5}$	138.11	27.09	133.35	-25.11	147.68
			C.M II	$A_{1.5}$	140.30	27.59	135.54	-20.99	147.52
		O₂	C.M I	A_3	104.29	19.99	99.55	-84.08	147.21
			C.M II	A_3	108.16	21.02	103.42	-75.53	146.24
	Dc.III	N₂	C.M I	A_2	157.68	28.71	152.53	-12.30	160.13
			C.M II	A_2	159.62	29.10	154.47	-9.02	160.04
		O₂	C.M I	A_2	127.00	22.54	121.84	-63.64	161.27
			C.M II	A_2	130.46	23.33	125.30	-57.05	160.64

Table 2 — Thermodynamic parameters of dehydration I (Dh. I, Dh II) and decomposition (Dc.I, Dc.II, Dc.III reactions)

	Reac.	Model		C. M I				C. M II			
		Atmospheric condition		R^2	S	E_a (kJ/mol)	KAS E_a (kJ/mol)	R^2	S	E_a (kJ/mol)	FWO E_a (kJ/mol)
Dehydration	Dh. I	N₂	A_2	0.99	12.57	65.88	76.87	0.99	11.86	67.61	78.09
			$A_{1.5}$	0.99	16.73	89.59		0.99	15.82	90.14	
		O₂	A_2	0.99	11.19	67.95	82.25	0.99	10.56	69.56	83.18
			$A_{1.5}$	0.99	14.89	92.33		0.99	14.08	92.74	
	Dh. II	N₂	A_4	0.94	10.99	51.27	54.92	0.95	10.54	54.04	57.55
			A_3	0.95	14.69	70.22		0.95	14.06	72.06	
		O₂	A_3	0.98	15.76	71.53	72.10	0.97	15.06	73.26	73.84
			A_4	0.97	11.80	52.26		0.97	11.30	54.94	
Decomposition	Dc. I	N₂	$A_{1.5}$	0.99	10.11	95.77	109.76	0.99	9.78	99.03	112.40
			R_2	0.99	12.78	125.49		0.99	12.32	127.29	
		O₂	$A_{1.5}$	0.99	16.20	78.57	82.85	0.99	15.64	82.74	86.85
			R_2	0.98	20.17	102.59		0.98	19.42	105.58	
	Dc. II	N₂	$A_{1.5}$	0.99	5.33	138.11	155.84	0.99	5.47	140.30	157.24
			R_2	0.98	6.24	179.16		0.99	6.42	178.98	
		O₂	A_3	0.98	15.27	104.29	114.72	0.98	14.71	108.16	118.03
			A_4	0.98	11.40	75.85		0.98	11.03	81.12	
	Dc. III	N₂	A_2	0.99	13.13	157.68	163.99	0.99	12.52	159.62	165.70
			$A_{1.5}$	0.99	17.52	213.64		0.99	16.69	212.83	
		O₂	A_2	0.94	5.256	127.00	151.17	0.95	5.15	130.46	153.50
			$A_{1.5}$	0.94	7.063	172.73		0.95	6.87	173.94	

consecutively and border separation of initial and final temperatures is too difficult. Firstly, the combination of three decomposition reactions were studied by using very small α values and Ea-α variation graphs were prepared (Fig. 4a). In nitrogen atmosphere, activation energies reach minimum

values at 0.465 and 0.610 decomposition ratios. These decomposition ratios change as 0.512 and 0.650 in oxygen atmosphere respectively. Temperature and time values at these decomposition ratios were used and reaction boundaries of the three consecutive reactions were determined precisely. After this procedure each stage of decomposition was reexamined. Activation energy values were calculated and the variations with respect to decomposition ratio, α, were graphed in Fig. 5.

Decomposition I (Dc.I) realizes endothermically and corresponds to formation of $Pb(CH_3COO)_2.PbO$ product in both atmosphere. Average activation energies of this reaction were calculated as 111.08 and 84.85 kJ/mol in nitrogen and oxygen atmospheres, respectively.

Decomposition II (Dc.II) occurs in a narrow temperature range (in nitrogen atmosphere: 542-592K and in oxygen atmosphere: 554-586K). The tendencies of the Ea-α variation graphs are different in both atmospheres. Initially activation energies increase persistently till to α =0.6 decomposition ratio (except α =0.20) and then decrease till to α =0.80 and finally increase again partially in nitrogen atmosphere. In oxygen atmosphere, the increasing of activation energies continue up to α =0.85 and after this decomposition ratio decrease slightly. Average activation energies are 156.54 and 116.38 kJ/mol in nitrogen and oxygen atmospheres respectively

Decomposition III (Dc.III) completes with 9.76% weight loss and shows endothermic character in nitrogen atmosphere. In this atmosphere activation
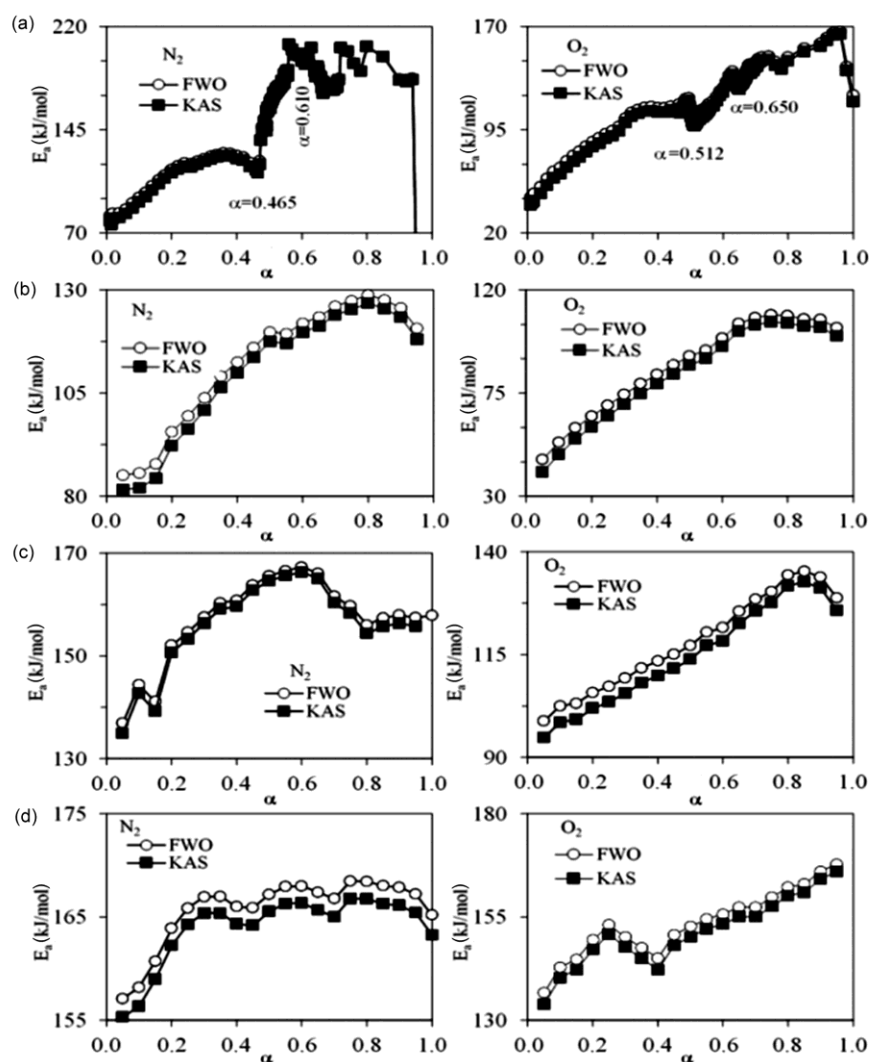
Fig. 5 — E_a-α variation graphs of decomposition reactions (a: combined decomposition reactions, b: decomposition I, c: decomposition II, d: decomposition III)

energy values show fluctuations with increasing decomposition ratio and average value is 164.84 kJ/mol. Same reaction completes with 8.74% weight loss in oxygen atmosphere. Reaction shows exothermic property due to the oxidation of PbO and formation of Pb_3O_4. Activation energy values increase with an increasing in the decomposition ratio up to α=025 then decrease in the α=0.25-0.40 range. After the α=0.40, the values of activation energy increase gradually. Average activation energy is calculated as 152.33 kJ/mol.

After the completion of these model-free calculations, reaction models of each decomposition stage were investigated by using C.M I and C.M. II methods. Standard deviations, regression analysis values and average activation energies which were calculated from the most two appropriate model were presented in Table 1. Same table includes activation energy values, which were calculated by using model free KAS and FWO equations, for comparison.

As seen from the Table 1, all decompositions fit in nucleation and growth model with different indexes. Nucleation model is used in the academic literature frequently in order to explain decomposition mechanism[35]. Gabal[24] investigated the thermal decomposition of cadmium and zinc oxalate mixture. Author calculated the activation parameters of each reaction stage with using the integral composite methods and stated that the reactions were best described by the random nucleation model. In addition decomposition reactions of $LiNiPO_4$, which advance with two stages, were announced by using nucleation models[36].

The thermodynamic parameters of activated complexes were calculated by using slope and intercept values of the most proper model graphs and given in Table 2. Similar to dehydration reactions, decomposition reactions may be interpreted as slow reactions due to the negative entropy values of activated complexes.

Conclusion

DTA-TG curves of $Pb(CH_3COO)_2.3H_2O$ in nitrogen and oxygen atmospheres show that decomposition advances with five stages. Dehydration reactions, which are first two stages, are not affected by atmospheric conditions. Decomposition reactions and final residues depend on the atmospheric conditions. In nitrogen atmosphere, decomposition terminates by the formation of PbO and small amount metallic Pb mixture. In oxygen atmosphere, PbO is formed primarily. Oxidation reaction takes place with the advancement of temperature and some PbO turns into Pb_3O_4. The mass increasing in the TG diagram proves oxidation reaction. The final residue is PbO and Pb_3O_4 mixture. These final residues were confirmed by using X-ray powder diffraction method. The boundaries of each reaction were distinguished by using not only TG curves, but also the using minimum points in the activation energy versus decomposition ratio graphs. The kinetic and thermodynamic parameters of the dehydration and decomposition reactions were calculated. It was found that, dehydration and decomposition reactions are compatible with the nucleation models in both atmospheres. All reactions have negative entropy values. This situation indicates that the arrangement degrees of the activated complexes are higher than the corresponding initial states. Positive Gibbs Free energy values of the activated complexes, show that all reactions do not occur spontaneously, and heat input must be provided initially. The knowledge of kinetic and thermodynamic data is very important in theoretical studies. Thus, these findings have significant implications which will guide to further studies on lead (II) acetate trihydrate. Besides, they will contribute to the solution of various scientific and practical problems such as the participation of solid phases.

References

1   Cetişli H, Çılgı G K & Donat R, *J Therm Anal Calorim*, 108 (2011) 1213.
2   Nakano M, Fujiwara T & Koga N, *J Phys Chem C*, 120 (2016) 8841.
3   Çılgı G K & Cetişli H, *J Therm Anal Calorim*, 98 (2009) 855.
4   Diefallah H M, *Thermochim Acta*, 202 (1992) 1.
5   Koga N & Tanaka H, *Thermochim Acta*, 303 (1997) 69.
6   Marciuš M, Ristic´ M, Ivanda M & Music S, *J Mol Struct*, 1044 (2013) 231.
7   Elmasry M A A, Gaber A & Khater E M H, *J Therm Anal Calorim*, 47 (1996) 757.
8   Malecka B, *J Therm Anal Calorim*, 78 (2004) 535.
9   Shi L, Xu Y & Li Q, *Cryst Growth Des*, 8 (2008) 3521.
10 Vatistas N & Cristofaro S, *Electrochem Commun*, 2 (2000) 334.

11 Ghasemi S, Mousavi M F, Karami H, Shamsipur M & Kazemi S H, *Electrochim Acta*, 52 (2006) 1596.

12 Johnson D, Feng J & Houk L, *Electrochim Acta*, 46 (2000) 323.

13 Zhou Y, Lin H, Gu Q, Long J & Wang X, *RSC Adv*, 33 (2012) 12624.

14 Mohamed M A, Halawy S A & Ebrahim M, *Thermochim Acta*, 236 (1994) 249.

15 Wendlant W W M, Thermal Analysis (Wiley & Sons, Incorporated John, New York) 3rd Ed. (1986).

16 Kissinger H E, *Anal Chem*, 29 (1957) 1702.

17 Ozawa T, *Bull Chem Soc Jpn*, 39 (1966) 2071.

18 Uzun N, Çolak A T, Emen F M & Çılgı G K, *J Therm Anal Calorim*, 124 (2016) 1735.

19 Akyurek Z & Coskun S, *Indian J Chem Technol*, 28 (2021) 473.

20 Sridevi B, Chitra M & Nalini Suja R, *Indian J Chem Technol*, 29 (2022) 729.

21 Balakrishnan R, Varghese L A & Manu S K, *Indian J Chem Technol*, 28 (2021) 336.

22 Budrugeac P & Segal E, *J Therm Anal Calorim*, 82 (2005) 677.

23 Huang Z, Wang X, Lu T, Nong D, Gao X, Zhao J, Wei M & Teng L, *J Therm Anal Calorim*, 140 (2020) 695.

24 Gabal M A *Thermochim Acta*, 412 (2004) 55.

25 Wang W H, Su W, Hu S Y, Huang Y, Pan Y, Chang S C & Shu C M, *J Therm Anal Calorim*, 147 (2022) 12019.

26 Zhang J, Guo Y, Shi L, Liu Q, Jiang S, Li Y & Li K, *J Therm Anal Calorim*, 147 (2022) 12201.

27 Çılgı G K, Cetişli H & Donat R, *J Therm Anal Calorim*, 110 (2012) 127.

28 Çılgı G K, Cetişli H & Donat R, *J Therm Anal Calorim*, 115 (2014) 2007.

29 The International Centre for Diffraction Data File No. 01-077-1971, 00-005-0561 and 03-065-2863.

30 The International Centre for Diffraction Data File No. 03-065-2851 and 01-077-1971.

31 Çılgı G K & Ak M, *J Mol Struct*, 1221 (2020) 128879.

32 Favergeon L, Pijolat M & Helbert C, *J Mater Sci*, 43 (2008) 4675.

33 Koga N & Tanaka H, *Thermochim Acta*, 388 (2002) 41.

34 Boonchom B, *J Therm Anal Calorim*, 98 (2009) 863.

35 Boonchom B & Danvirutai C, *J Therm Anal Calorim*, 98 (2009) 771.

36 Galwey A K, *React Kinet Mech Catal*, 114 (2014) 1.

37 He Y, Liao S, Chen Z, Li Y, Xia Y, Wu W & Li B, *J Therm Anal Calorim*, 115 (2014) 237.